arXiv:1402.1833v1 [cond-mat.supr-con] 8 Feb 2014

Observation of anomalous temperature dependence of spectrum on small Fermi surfaces in a BiS_2-based superconductor

L. K. Zeng[1], X. B. Wang[1], J. Ma[1], P. Richard[1,2], S. M. Nie[1], H. M. Weng[1], N. L. Wang[1,2], Z. Wang[3], T. Qian[1],* and H. Ding[1,2]†
[1]*Beijing National Laboratory for Condensed Matter Physics, and Institute of Physics, Chinese Academy of Sciences, Beijing 100190, China*
[2]*Collaborative Innovation Center of Quantum Matter, Beijing, China and*
[3]*Department of Physics, Boston College, Chestnut Hill, Massachusetts 02467, USA*

We have performed an angle-resolved photoemission spectroscopy study of the BiS_2-based superconductor Nd(O,F)BiS_2. Two small electron-like Fermi surfaces around X (π, 0) are observed, which enclose 2.4% and 1.1% of the Brillouin zone area, respectively, corresponding to an electron doping of 7% per Bi site. The low-energy spectrum consists of a weakly-dispersing broad hump and a dispersive branch, which follows well the calculated band dispersion. This hump is drastically suppressed with increasing temperature, while the dispersive branch is essentially unaffected. The anomalous thermal effect indicates a highly interacting electronic state, in which the superconducting pairing develops.

PACS numbers: 74.25.Jb, 71.18.+y, 74.70.-b, 71.38.-k

The recent discovery of superconductivity with T_c up to ~ 10 K in the BiS_2-based compounds has attracted a lot of attentions [1–10]. As in the cuprate and iron-based high-T_c superconductors, the BiS_2 family has a layered crystal structure consisting of superconducting BiS_2 layers intercalated with various block layers. Band structure calculations show that the parent compound of the BiS_2-based superconductors is a band insulator with an energy gap of ~ 0.8 eV [11–14], and bulk superconductivity induced by electron doping is derived from the Bi $6p_x/p_y$ orbitals, in which correlation effects are expected to be weaker than those in the 3*d* orbitals of the cuprate and iron-based superconductors. The superconducting transition temperature T_c reaches a maximum at a nominal doping level $\delta \sim 0.5$ for many compounds [1–10], where strong nesting between the large parallel Fermi surface (FS) segments is suggested in band calculations [11–14]. Therefore, most of the theoretical models for the pairing mechanism are based on the nesting scenario.

However, there is a large bifurcation regarding the consequences of the nesting. On the one hand, the nesting is proposed to enhance the electron-phonon coupling, thus favoring a conventional BCS superconductivity [11–14]. On the other hand, as widely believed for the iron-based superconductors, the strong FS nesting could enhance charge or spin fluctuations, and thus electronic correlations may play a major role in the superconducting pairing [15–18]. Magnetic penetration depth and muon-spin rotation spectroscopy measurements support a conventional *s*-wave superconductivity in the strong electron-phonon coupling limit [19, 20], whereas the absence of phonon anomaly in neutron scattering measurements suggests that the electron-phonon coupling may be much weaker than theoretically expected [21]. Recent scanning tunneling spectroscopy measurements show that the ratio $2\Delta/k_BT_c$ is much larger than the BCS value [22, 23]. Giant superconducting fluctuations and an anomalous semiconducting normal state are also observed, suggesting that the superconductivity might be different from that of a conventional BCS superconductor [23].

In this Letter, we present angle-resolved photoemission spectroscopy (ARPES) results of the BiS_2-based superconductor Nd(O,F)BiS_2 (T_c^{zero} = 4 K). Two small electron-like FSs around X (π, 0) are observed, corresponding to an electron doping of 7% of itinerant carriers per Bi site. As a result, the measured electronic structure is far from the proposed FS nesting. Furthermore, we reveal that the low-energy spectrum consists of a broad hump around -0.3 eV, which is drastically suppressed with increasing temperature, and a dispersive branch, which is essentially unaffected by the temperature. This exotic spectral behavior suggests that the low-temperature normal state of this superconductor is a highly interacting electronic state.

Single crystals with a nominal composition of $NdO_{0.7}F_{0.3}BiS_2$ were grown by a flux method with KCl/LiCl as the flux. Energy dispersion spectrum (EDS) measurements were performed on several pieces of samples, which give an averaged composition of $Nd_{0.95\pm0.02}O_yF_{0.44\pm0.1}Bi_{0.94\pm0.02}S_2$. ARPES measurements were performed at the Institute of Physics, Chinese Academy of Sciences, using the He Iα ($h\nu$ = 21.218 eV) resonance lines. The angular and energy resolutions were set to 0.2° and 14 ~ 32 meV, respectively. Samples with a typical size of ~ 1 × 1 mm^2 were cleaved *in situ* at 30 K and measured between 30 and 230 K in a working vacuum better than 4×10^{-11} Torr. The Fermi level (E_F) of the samples was referenced to that of a gold film evaporated onto the sample holder.

Figure 1 shows the band dispersions along the high-symmetry lines Γ-M-X-Γ in an energy range within 4 eV below E_F. We observe several dispersive bands below -1.2 eV and an electron-like band dispersion with a bottom of -0.3 eV near X. There is an energy gap of ~ 0.9 eV between them. To understand the multiband electronic structure, we superimpose the local-density approximation (LDA) band structure on top of our data. The calculated band structure reflects some main features in the experiment data, especially for the direct gap between the conduction and valence bands. In LDA calculations, the undoped parent compound is a band insulator and

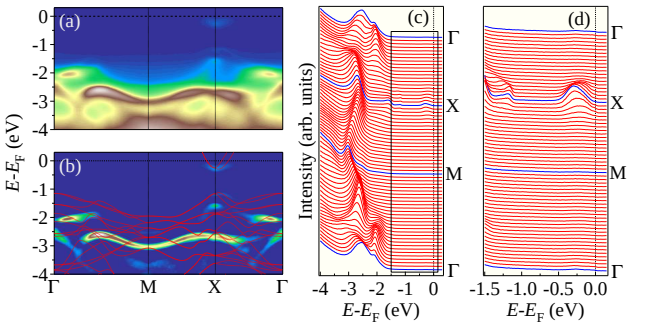


FIG. 1. (Color online) (a) ARPES intensity plot along the high symmetry lines Γ-M-X-Γ taken at 30 K. Γ-X is along the nearest Bi-Bi direction. (b) Corresponding two-dimensional curvature intensity plot. LDA bands without SOC for the undoped parent compound $LaOBiS_2$, which are essentially the same as those of $NdOBiS_2$ in the energy in our experiments, are also plotted in (b) for comparison. E_F of the calculated band structure is set to be 1.15 eV above the top of the valence bands to match the experimental band dispersions. (c) Corresponding EDCs. (d) Magnification of the box in (c).

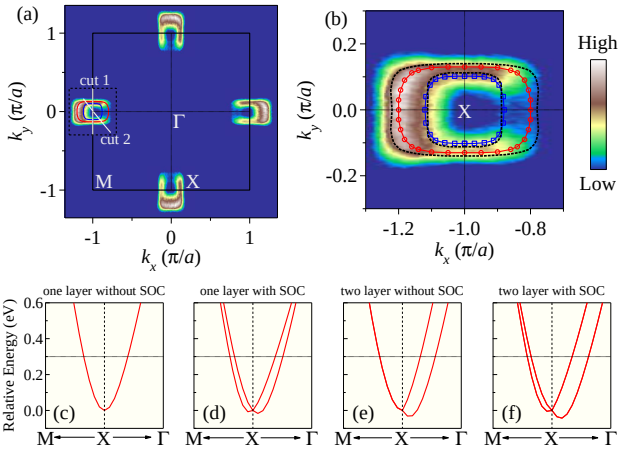


FIG. 2. (Color online) (a) ARPES intensity plot at E_F as a function of the two-dimensional wave vector taken at 30 K. The intensity is obtained by integrating the spectra within ±15 meV with respect to E_F. The data are symmetrized by assuming a fourfold symmetry with respect to Γ. Red and blue lines represent the extracted FSs. White lines labeled cut1 and cut2 indicate the momentum locations, along which the data are shown in Figs. 3 and 4, respectively. (b) Magnification of the dashed box in (a). Circles and squares show the experimentally determined k_F points. Dashed black lines represent the LDA + SOC calculated FSs. (c) and (d) Calculated conduction bands at X using one-BiS_2-layer models with and without SOC, respectively. (e) and (f) Same as (c) and (d), respectively, but using two-BiS_2-layer models. In (c)-(f), the zero energy is defined to the band bottom at X and the horizontal dashed lines at 0.3 eV represent the approximate position of E_F.

its E_F is located within the energy gap. The experimentally obtained E_F is situated in the conduction bands, indicating that electron carriers are introduced in the superconducting samples due to the substitution of O with F.

Figure 2 shows the FS mapping data in the k_x-k_y plane. We extract two FS pockets centered at X, which come from the near-E_F electron-like dispersion shown in Fig. 1. The two extracted FSs exhibit a significantly anisotropic separation, which is a result of the cooperative effects from spin-orbit coupling (SOC) and interlayer coupling, as explained below. We have performed LDA calculations using the following models. In a one-BiS_2-layer model (same as the surface layer after cleave) with SOC [Fig. 2(d)], the near-E_F bands are split along both XM and ΓX with comparable magnitudes. In a two-BiS_2-layer model (same as the bulk) without SOC [Fig. 2(e)], the bands are doubly-degenerate along XM, but split along ΓX due to the interlayer coupling. In the presence of SOC, the Rashba term lifts the degeneracy along XM but the splitting magnitude along XM is much smaller than along ΓX [Fig. 2(f)], in agreement with our observations.

The two FS pockets enclose 1.1% and 2.4% of the Brillouin zone area, respectively. Counting the Luttinger volume of two-dimensional FS sheets, the two observed FSs correspond to an electron doping of 7% per Bi site. The value for doped itinerant carrier density is much less than those inferred from the nominal composition and the EDS data. The discrepancy can be explained in several ways. Firstly, the possibility of charge polarization at the terminal layer cannot be completely excluded, though this scenario is unlikely since the cleavage occurs between two symmetrical BiS_2 layers. Moreover, the plasma frequency calculated using the experimental doping level is ~ 2.1 eV, in agreement with the optical data [24], suggesting that the ARPES data reflect the intrinsic carrier density in the bulk. Secondly, as both oxygen and fluorine are light elements, their concentrations given from the EDS data may not be reliable [23]. Thirdly, part of the carriers may be localized and thus do not contribute to the conduction band. In this case, the localized carriers could form flat bands within the energy gap.

We find that at low temperature, the low-energy spectrum near E_F consists of a large hump around -0.3 eV and a dispersive branch, which tracks well the calculated conduction band dispersion. Figure 3 shows ARPES data of the conduction bands taken along XM at 30 K. Two electron-like bands are resolved in Figs. 3(b) and 3(d). As mentioned above, the band splitting along XM originates from the SOC. The band dispersion, extracted by tracking the peak positions of the momentum distribution curves (MDCs), follows well the LDA bands calculated with SOC. On the other hand, the energy distribution curves (EDCs) are characterized by a broad hump, whose maximum does not cross E_F but tends to bend back beyond k_{F2} [Fig. 3(c)]. As shown in Fig. 3(e), the EDC at k_{F2} shows a sharp Fermi cutoff, indicating a metallic behavior. There is a change of the slope on the lower binding energy side of the hump at ~ -0.05 eV. The linear extrapolation suggests that the hump contributes vanishingly small spectral weight at E_F, indicating that the finite low-energy spectral weight at E_F is dominated by the dispersive branch.

The low-energy spectrum shows anomalous temperature

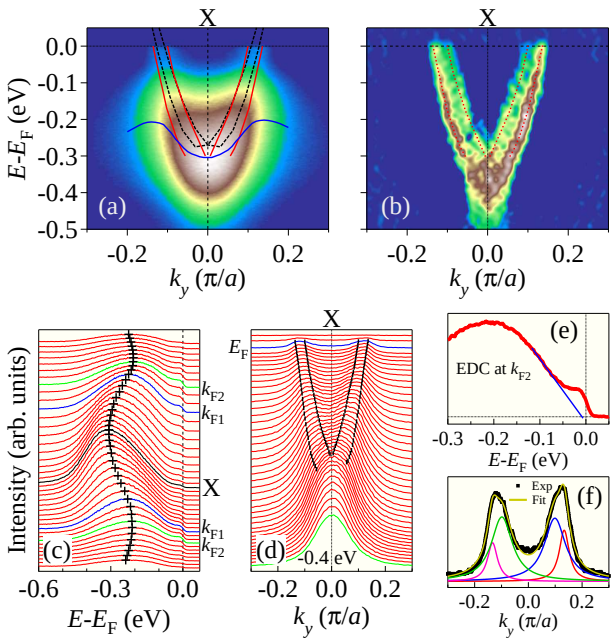


FIG. 3. (Color online) (a) ARPES intensity plot along XM (cut 1 from Fig. 2(a)) taken at 30 K. Red and blue lines represent the dispersions extracted from the peak positions of the MDCs and EDCs, respectively. Dashed black lines represent the LDA + SOC calculated bands. (b) Corresponding intensity plot of second derivative along momentum. Dotted lines are the same as the red lines in (a). (c) Corresponding EDCs. Crosses indicate the peak positions of the EDCs. Black, blue and green curves represent the EDCs at X, k_{F1} and k_{F2}, respectively. k_{F1} and k_{F2} represent the Fermi wave vectors of the inner and outer electron-like bands, respectively. (d) Corresponding MDCs. Short verticals indicate the peak positions of the MDCs. Blue and green curves represent the MDCs at E_F and -0.4 eV, respectively. (e) EDC at k_{F2}. Blue line represents a linear extrapolation of the slope on the lower binding energy side of the hump. (f) MDC at E_F. The MDC is fitted to four Lorentzian peaks, indicating the band splitting along XM due to SOC.

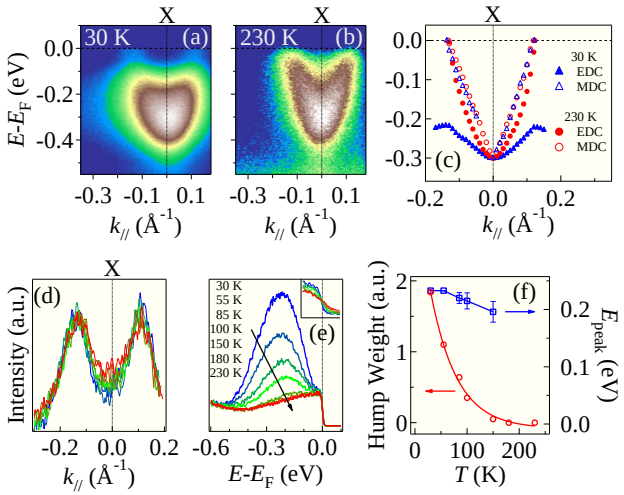


FIG. 4. (Color online) (a) and (b) ARPES intensity plots through the X point (cut 2 from Fig. 2(a)) taken at 30 and 230 K, respectively. (c) E-k plot of the positions of the EDC and MDC peaks taken at 30 and 230 K, respectively. To approximately remove the effect of the Fermi function on the EDC peak position near E_F, the EDC peak positions are extracted from the symmetrized curve with respect to E_F. (d) and (e) MDCs at E_F and EDCs at k_F of the left branch taken at various temperatures between 30 and 230 K, respectively. Thermal broaden effect on the EDCs in (e) is removed (see text for details). Inset of (e) plots the EDCs (raw data) in a energy window of [-0.05, 0.05 eV]. (f) Spectral weight (left axis) and binding energy of the maximum (right axis) of the broad hump against temperature. The spectral weight is obtained by subtracting the integration of the EDC at 230 K from that taken at the corresponding temperature.

dependence characterized by a rapid suppression of the spectral weight of the broad hump with increasing temperature that, nevertheless, leaves the dispersive branch little changed. The temperature dependent ARPES results along cut 2 are shown in Fig. 4. A sharp contrast between the intensity contours at 30 K [Fig. 4(a)] and 230 K [Fig. 4(b)] is clearly visible. To further clarify the evolution of the spectrum with temperature, we plot the MDCs at E_F and the EDCs at k_F of the left branch at various temperatures between 30 and 230 K in Figs. 4(d) and 4(e), respectively. All the spectra are normalized by the photon flux. To remove the thermal broadening effect due to the Fermi-Dirac statistics, the EDCs in Fig. 4(e) are divided by the resolution-convoluted Fermi functions at corresponding temperatures and then multiplied by that of 10 K. The MDCs almost collapse onto a single curve, whereas the lineshape of the EDCs changes dramatically with temperature. The spectral weight of the broad hump is suppressed rapidly with increasing temperature. The hump can no longer be clearly resolved above 150 K and the spectra at 180 K and 230 K nearly coincide. In sharp contrast to the loss of spectral weight below E_F, the Fermi cutoff of all the EDCs (raw data) taken at various temperatures crosses exactly at E_F [inset of Fig. 4(e)], which is consistent with the collapse of the MDCs shown in Fig. 4(d), indicating a negligible temperature effect on the spectral weight at E_F that is dominated by the dispersive branch. As shown in Fig. 4(c), with the suppression of the broad hump, the dichotomy between the dispersions of EDC and MDC peaks is almost eliminated at 230 K. The dispersions at 230 K are in good consistence with the one extracted from the MDCs at 30 K that corresponds to the dispersive branch. Therefore, in sharp contrast to the strong temperature dependence of the broad hump, the dispersive branch is essentially unaffected with temperature.

A conventional explanation for temperature-induced loss of spectral weight is through the effect of lattice vibrations. Such an effect in photoemission spectra is similar to that found in X-ray and neutron scattering, where the intensities of diffraction peaks are multiplied by the Debye-Waller factor e^{-2W} ($W \propto T$) [25]. Indeed, the integrated spectral weight as a function of temperature can be approximately fitted to a function of $A + Be^{-CT}$, as shown in Fig. 4(f). However, the extracted Debye temperature from the fitting is about only 3 K [26], two orders of magnitudes smaller than the estimated values from the specific heat data [6, 7, 27–29]. Therefore, the effect of

conventional lattice vibrations cannot explain the giant temperature effects in our data.

Loss of spectral weight over a large energy scale has been observed in a polaronic state of the colossal magnetoresistant manganites $La_{2-2x}Sr_{1+2x}Mn_2O_7$ [30–33]. In the polaronic state induced by strong electron-phonon coupling, the spectral function consists of a low-energy "zero-phonon" quasiparticle peak and a hump-like high-energy incoherent resonance. Our observation of a high-energy hump as well as a sharp Fermi cutoff bears some resemblance to the signature of polarons. In the manganites, the incoherent branch loses its partial spectral weight over an energy range of up to 0.8 eV, which is accompanied by a disappearance of the quasiparticle peaks around the metal-insulator transition temperature. This could be associated with either the loss of polaron coherence [32] or a decreased fraction of metallic regions in the scenario of phase separation [31]. Assuming that the polaron picture could be applied to the BiS_2 system, the spectral weight of the incoherent branch, *i.e.* the broad hump, is drastically suppressed with increasing temperature, while the low-energy coherent branch, which dominates the spectral weight at E_F, is not affected. The behavior looks very unusual in the framework of polarons because the strong suppression of the incoherent branch indicates significant changes of the polaronic states, which seems not to be perceived by the coherent part. Our spectra exhibit distinctly different temperature dependence from those in the manganites, indicating that the giant thermal effects observed in the two systems might have different origins.

The disorder-induced self-traping of polarons in $Na_{0.025}WO_3$ also shows nontrivial temperature dependence of the spectral function [34, 35]. The Na_xWO_3 and BiS_2 systems bear an interesting resemblance in their electronic structures. Their undoped parent compounds are band insulators with energy gaps of an order of eV between the valence and conduction bands. The introduction of electron carriers by element substitutions or intercalations leads to an insulator-metal transition on small electron-like FSs. The conduction electrons in $Na_{0.025}WO_3$ are self-trapped due to strong disorder induced by the randomly distributed Na^+ ions, forming a weakly dispersive polaron band near the top of valence bands. The breakdown of polarons at high temperature leads to a large decrease in the intensity of the polaron band, while the spectrum of the conduction band is not significantly changed. These properties are quite similar to what we have observed in BiS_2 except that the polaron band would be localized near the bottom of the conduction bands in our case. We note that the polaronic self-trapping of carriers could also explain the small FS pockets observed in our experiment. It is expected that as the polarons become more delocalized, the spectral weight should be transferred to other k-points. However, such a spectral weight transfer is not observed at least along the measured momentum cut.

In summary, our ARPES results show two small electron-like FSs around X (π, 0) instead of large hole-like FSs centered at Γ (0, 0) and M (π, π) proposed in recent theoretical models. The anomalous temperature dependence of the low-energy spectrum indicates that the superconducting pairing develops in a highly interacting electronic state. Our results provide detailed information on the low-energy electronic structures and valuable insights for further experimental and theoretical studies of the pairing mechanism in the BiS_2-based superconductors.

We acknowledge X. Dai and Z. Fang for valuable discussions. This work was supported by grants from CAS (2010Y1JB6), MOST (2010CB923000, 2011CBA001000, 2011CB921701, 2013CB921700, 2011CBA00108, and 2012CB821403), NSFC (11004232, 11050110422, 11274362, 11234014, 11120101003, 11074291, 11274359, and 11104339), and DOE (DE-FG02-99ER45747 and DE-SC0002554).

* tqian@iphy.ac.cn
† dingh@iphy.ac.cn

[1] Y. Mizuguchi, H. Fujihisa, Y. Gotoh, K. Suzuki, H. Usui, K. Kuroki, S. Demura, Y. Takano, H. Izawa, and O. Miura, Phys. Rev. B **86**, 220510(R) (2012).
[2] S. K. Singh, A. Kumar, B. Gahtori, Shruti, G. Sharma, S. Patnaik, and V. P. S. Awana, J. Am. Chem. Soc. **134**, 16504 (2012).
[3] Y. Mizuguchi, S. Demura, K. Deguchi, Y. Takano, H. Fujihisa, Y. Gotoh, H. Izawa, and O. Miura, J. Phys. Soc. Jpn. **81**, 114725 (2012).
[4] S. Demura, Y. Mizuguchi, K. Deguchi, H. Okazaki, H. Hara, T. Watanabe, S. J. Denholme, M. Fujioka, T. Ozaki, H. Fujihisa, Y. Gotoh, O. Miura, T. Yamaguchi, H. Takeya, and Y. Takano, J. Phys. Soc. Jpn. **82**, 033708 (2013).
[5] J. Xing, S. Li, X. Ding, H. Yang, and H. H. Wen, Phys. Rev. B **86**, 214518 (2012).
[6] X. Lin, X. X. Ni, B. Chen, X. F. Xu, X. X. Yang, J. H. Dai, Y. K. Li, X. J. Yang, Y. K. Luo, Q. Tao, G. H. Cao, and Z. A. Xu, Phys. Rev. B **87**, 020504(R) (2013).
[7] D. Yazici, K. Huang, B. D. White, I. Jeon, V. W. Burnett, A. J. Friedman, I. K. Lum, M. Nallaiyan, S. Spagna, and M. B. Maple, Phys. Rev. B **87**, 174512 (2013).
[8] K. Deguchi, Y. Mizuguchi, S. Demura, H. Hara, T. Watanabe, S. J. Denholme, M. Fujioka, H. Okazaki, T. Ozaki, H. Takeya, T. Yamaguchi, O. Miura, and Y. Takano, Europhys. Lett. **101**, 17004 (2013).
[9] S. Demura, K. Deguchi, Y. Mizuguchi, K. Sato, R. Honjyo, A. Yamashita, T. Yamaki, H. Hara, T. Watanabe, S. J. Denholme, M. Fujioka, H. Okazaki, T. Ozaki, O. Miura, T. Yamaguchi, H. Takeya, and Y. Takano, arXiv:1311.4267
[10] R. Jha and V. P. S. Awana, arXiv:1401.4811
[11] H. Usui, K. Suzuki, and K. Kuroki, Phys. Rev. B **86**, 220501(R) (2012).
[12] X. G. Wan, H. C. Ding, S. Y. Savrasov, and C. G. Duan, Phys. Rev. B **87**, 115124 (2013).
[13] B. Li, Z. W. Xing, and G. Q. Huang, Europhys. Lett. **101**, 47002 (2013).
[14] T. Yildirim, Phys. Rev. B **87**, 020506(R) (2013).
[15] T. Zhou and Z. D. Wang, J. Supercond. Novel Magn. **26**, 2735 (2013).
[16] G. B. Martins, A. Moreo, and E. Dagotto, Phys. Rev. B **87**, 081102(R) (2013).

[17] Y. Yang, W. S. Wang, Y. Y. Xiang, Z. Z. Li, and Q. H. Wang, Phys. Rev. B **88**, 094519 (2013).
[18] Y. Liang, X. X. Wu, W. F. Tsai, and J. P. Hu, arXiv:1211.5435
[19] G. Lamura, T. Shiroka, P. Bonfa, S. Sanna, R. De Renzi, C. Baines, H. Luetkens, J. Kajitani, Y. Mizuguchi, O. Miura, K. Deguchi, S. Demura, Y. Takano, and M. Putti, Phys. Rev. B **88**, 180509(R) (2013).
[20] Shruti, P. Srivastava, and S. Patnaik, J. Phys.: Condens. Matter **25**, 339601 (2013).
[21] J. Lee, M. B. Stone, A. Huq, T. Yildirim, G. Ehlers, Y. Mizuguchi, O. Miura, Y. Takano, K. Deguchi, S. Demura, and S. H. Lee, Phys. Rev. B **87**, 205134 (2013).
[22] S. Li, H. Yang, D. Fang, Z. Wang, J. Tao, X. Ding, and H. H. Wen, Sci. China-Phys. Mech. Astron. **56**, 2019 (2013).
[23] J. Z. Liu, D. L. Fang, Z. Y. Wang, J. Xing, Z. Y. Du, X. Y. Zhu, H. Yang, and H. H. Wen, arXiv:1310.0377
[24] X. B. Wang and N. L. Wang (unpublished)
[25] S. Hüfner, *Photoelectron Spectroscopy: Principles and Application* (Springer-Verlag, New York, 1995).
[26] In the calculation, Δk is defined to be (0, 0, $2\pi/c$).
[27] H. Takatsu, Y. Mizuguchi, H. Izawa, O. Miura, and H. Kadowaki, J. Phys. Soc. Jpn. **81**, 125002 (2012).
[28] R. Jha, A. Kumar, S. K. Singh, and V. P. S. Awana, J. Appl. Phys. **113**, 056102 (2013).
[29] D. Yazici, K. Huang, B. D. White, A. H. Chang, A. J. Friedman, M. B. Maple, Philos. Mag. **93**, 673 (2013).
[30] S. de Jong, Y. Huang, I. Santoso, F. Massee, R. Follath, O. Schwarzkopf, L. Patthey, M. Shi, and M. S. Golden, Phys. Rev. B **76**, 235117 (2007).
[31] Z. Sun, J. F. Douglas, A. V. Fedorov, Y. D. Chuang, H. Zheng, J. F. Mitchell, and D. S. Dessau, Nature Phys. **3**, 248 (2007).
[32] N. Mannella, W. L. Yang, X. J. Zhou, H. Zheng, J. F. Mitchell, J. Zaanen, T. P. Devereaus, N. Nagaosa, Z. Hussain, and Z. X. Shen, Nature **438**, 474 (2005).
[33] N. Mannella, W. L. Yang, K. Tanaka, X. J. Zhou, H. Zheng, J. F. Mitchell, J. Zaanen, T. P. Devereaux, N. Nagaosa, Z. Hussain, and Z. X. Shen, Phys. Rev. B **76**, 233102 (2007).
[34] S. Raj, D. Hashimoto, H. Matsui, S. Souma, T. Sato, T. Takahashi, D. D. Sarma, P. Mahadevan, and S. Oishi, Phys. Rev. Lett. **96**, 147603 (2006).
[35] S. Raj, T. Sato, S. Souma, and T. Takahashi, Mod. Phys. Lett. B **23**, 2819 (2009).